Field Monitoring and Simulation of a Historic Mass Masonry Building Retrofitted with Interior Insulation

Kohta Ueno
Associate Member ASHRAE

John Straube, PhD, PEng
Associate Member ASHRAE

Randy Van Straaten
Student Member ASHRAE

ABSTRACT

Load-bearing masonry buildings are a significant portion of the existing building stock, and there is a great deal of interest in adding thermal insulation to the walls of these structures. Exterior insulation provides the ideal conditions for building durability; however, many buildings cannot be retrofitted with insulation on the exterior for reasons such as historic preservation, aesthetics, zoning, or space restrictions. Adding insulation to the interior side of walls of such masonry buildings in cold, and particularly cold and wet, climates may increase risks of performance and durability problems.

A circa 1917 construction mass masonry building located on a Boston-area university campus was retrofitted with interior polyurethane spray foam insulation. Sensors were installed in the retrofitted walls to measure temperature and moisture conditions within the assembly; interior and exterior boundary conditions were also monitored. Experimental variables included orientation, spatial location of monitoring, and assembly type (insulated experimental versus uninsulated control). Hygrothermal simulations were run on the original and retrofitted assemblies using measured site environmental data, both to assess durability risks, and for comparison with the measured data.

Measured data indicated that the insulated masonry walls were colder and had higher moisture contents than uninsulated assemblies, as would be expected. Hygrothermal simulations had good correlation to temperature measurements, but moisture measurements were less consistent. These differences may be due to sensor response, driving rain exposure, or anomalies within the mass masonry wall assembly. The simulations indicated a low risk of freeze-thaw damage.

The effect of thermal bridging through structural elements (uninsulated floor slabs) was examined with cold weather infrared thermography.

INTRODUCTION

Load-bearing mass masonry buildings are a significant portion of the existing building stock in the East Coast and Midwest regions of the United States. Continued use of these buildings (as opposed to demolition) retains the historic character of the building and its associated neighborhood, and utilizes the embodied energy built into these structures. However, in cold climates the need for improved energy performance and greater requirements for occupant comfort are motivations to retrofit insulation in these buildings. The thermal resistance of even thick masonry walls is far below modern code requirements: common moderate density brickwork (80 to 110 lb/ft^3 or 1280–1760 kg/m^3) can be assumed to provide an R-value from R-0.25 to R-0.33 per inch (k ≈ 0.43 to 0.58 W/[m·K]). Even at a thickness of 12–16 in. (0.3–0.4 m), this only provides insulation levels of R-3 to R-5 (RSI 0.5–0.9). The use of hollow clay block may add an additional R-1 to R-2 (RSI 0.1 to 0.4).

However, adding insulation to the interior side of walls of such masonry buildings in cold—and particularly cold and wet—climates has the potential to cause or accelerate performance and durability problems. These issues include freeze-thaw damage of the masonry wall, corrosion of embedded metal elements, and potential moisture damage to wood struc-

tural members embedded in the masonry. Exterior insulation provides the ideal conditions for building durability; however, many buildings cannot be retrofitted with insulation on the exterior for reasons such as historic preservation, cost, zoning or space restrictions, or aesthetics.

The authors worked with a Boston-area academic institution that owns a large inventory of existing mass masonry buildings. This institution has been moving into capital renovation projects which include the retrofit of interior insulation; to gain a greater understanding of the potential risks, the institution implemented wall monitoring on an initial project. The intent was that the data collected from this site would be used to inform upcoming projects, including the magnitude of potential risks. This work covers the instrumentation, collected data, and analysis of this masonry insulation retrofit project.

BACKGROUND AND PREVIOUS WORK

An overview of the building physics and durability risks associated with interior insulation of mass masonry buildings is covered by Straube and Schumacher (2007). Interior insulation reduces heat flow through the assembly, thus changing the existing moisture balance of wetting and drying. Given this reduced drying, the retrofit design should reduce wetting in a commensurate manner. The winter temperatures of parts of the inner layers of masonry are also significantly lowered, thereby raising the risk of freeze-thaw damage. The document covers the risks associated with interior-sourced air leakage condensation; this problem is likely when fibrous air permeable (e.g., fiberglass batt) insulation is used with an inadequate interior air barrier. This is a particular problem if the insulation is not applied tightly to the masonry wall, resulting in an air space which allows convective looping. A preferred approach, instead, is to use air impermeable, vapor semi-permeable spray foam, which can achieve airtightness levels required to avoid condensation issues.

Wilkinson et al. (2009) installed wall instrumentation in a circa 1950 retrofitted mass masonry three-story building, located in Toronto, Ontario, Canada; their data compared the performance of insulated and non-insulated wall sections. Wilkinson also provided a review of the current relevant literature, including case studies showing good durability of buildings with interior insulation retrofits, guidance on methods to minimize risks in retrofit design, and specific durability concerns raised during retrofits (freeze-thaw damage of masonry and corrosion of embedded metal components). One conclusion was the fact that although the brick would not meet modern freeze-thaw performance standards, the retrofitted wall had low freeze-thaw deterioration risk (based on both monitored data and simulations). Monitored data suggested that there might be a minor increase in embedded metal corrosion risk, but simulations indicated no added risk; this was ascribed to an artifact of the sensor measurements. Another conclusion was that the embedded wall moisture sensors used were not suitable for detecting moisture contents in the range causing freeze-thaw risk; slow sensor time response also reduced the utility of these sensors.

Mensinga et al. (2010) and Lstiburek (2010) describe masonry material property testing that provides better prediction of freeze-thaw resistance than currently used methods, such as the cold soak/boil ratio or saturation coefficient (ASTM 2012) and rapid freeze thaw (ASTM 2008). The metric used in the recent work is the critical degree of saturation (Fagerlund 1977), or S_{crit}; masonry can experience unlimited freeze-thaw cycling below this critical moisture content without damage, while above this moisture level, damage will occur quickly. Unlike previous methods, which are simple pass/fail criteria (suitable versus unsuitable for exposure), this metric results in a limit state design process for assessing the retrofit risk of the assembly. The measured S_{crit} is used as a risk threshold in hygrothermal simulations; local climate conditions, building exposures, and enclosure design are used as inputs to determine the durability risk associated with the retrofit of interior insulation.

Straube et al. (2012) provides an overview of the topic of interior insulation retrofits of mass masonry buildings. The document includes background on the building physics and potential durability risks, and presents a variety of recommended (and non-recommended) interior retrofit assemblies. This is followed by guidance on problematic details, typically linked with water concentrations on the face of the building, and methods to reduce the moisture loading. The final section provides steps to mitigate risk in these retrofits, including site assessment of the building, various material property tests and computer simulations, site assessment of the driving rain loads, monitoring of prototype insulated assemblies, and recommendations for ongoing post-retrofit maintenance and repair of the building.

SITE DESCRIPTION AND MONITORING PACKAGE

A research project was initiated by a Boston-area academic institution to monitor the in-situ hygrothermal performance of a mass masonry building retrofitted with interior insulation. The test site for this research is the Arthur D. Little Building, which is a three-story (with basement) building (overviews in Figure 1; close up of north and south façades in Figure 2) located in Cambridge, MA (DOE Zone 5A). The building was constructed in 1917, and is on the National Historic Register. The structural elements are site-cast reinforced concrete; the existing walls included (from exterior to interior) face brick, fill brick, hollow clay block, an asphalt-based dampproofing coating, and a direct-applied cementitious interior plaster rendering (see Figure 3 for representative wall sections). A major renovation project in 2010–2011 included the installation of insulation on the interior side of the mass masonry assembly. The interior plaster was removed, and open cell polyurethane spray foam (ocSPF) was applied to the interior face of the masonry wall. Insulation was approximately 3 to 3 ½ in. (75 to 90 mm) thick, partially encasing the 2 ½ in. (63.5 mm) steel studs, which were spaced approximately 1 ¾ in. (44 mm) off the masonry wall. This interior wall retrofit assembly addresses air leakage condensation risks; spacing the framing members off the wall reduces the impact of thermal bridging associated with the steel studs. The overall R-value

Figure 1 *Exterior views of the Arthur D. Little Building (left to right): front/south elevation, partial rear/north elevation, and overhead rendering from the south, showing surroundings.*

Figure 2 *South (front) and north (rear) monitoring locations and wall type nomenclature.*

of the retrofit assembly is in the R-10.6 (RSI 1.9) range, using algorithms from Kosny and Christian (1995). The building was occupied in late 2011; the building's primary function is office space.

Wall Designations and Nomenclature

The wall instrumentation has been clustered into the following test walls; they are shown on the building elevation in Figure 2. Instrumentation was installed on north and south orientations; project north and south are the rear and front elevations of the building, respectively; actual orientations are 335° and 155°. Greater emphasis was placed on the north-facing walls, given the colder conditions, which results in greater risks of freeze-thaw damage.

- South 1 ("Thin" Wall): The walls that surround the window openings are roughly 12 in. (305 mm) thick and are composed of three layers (interior hollow core clay block, fill brick, and face brick; see Figure 3).
- South 2 ("Thick" Wall): At the main body of the wall or pilasters between windows, the masonry wall is thicker, with two fill brick layers instead of one, resulting in a wall thickness of approximately 17 in. (430 mm).

- North 1 ("Thin" Wall): As per south side, at analogous location.
- North 2 ("Thick" Wall): As per south side, at analogous location.
- North 3 ("False Parapet"): Given the higher rain exposure at the top of the building, additional instrumentation was installed high on the walls, above the third floor's finish ceiling. Note that this building does not have an actual parapet (roof slab is cast directly on top of the wall); however, this "false parapet" space has high exposure to rain.
- North 4 (Uninsulated): The rear service stairwell has been left uninsulated; therefore, it provides an opportunity to compare the behavior of walls with and without insulation, but with similar exposure. The other remaining walls are insulated. One problem with the installation was that the instrumentation was installed in a location that is sheltered from rain by the roof cornice detail, due to interior details (stairwell landing). In addition, stairwell temperature conditions were not as tightly controlled as interior main space setpoints, including no summertime cooling.
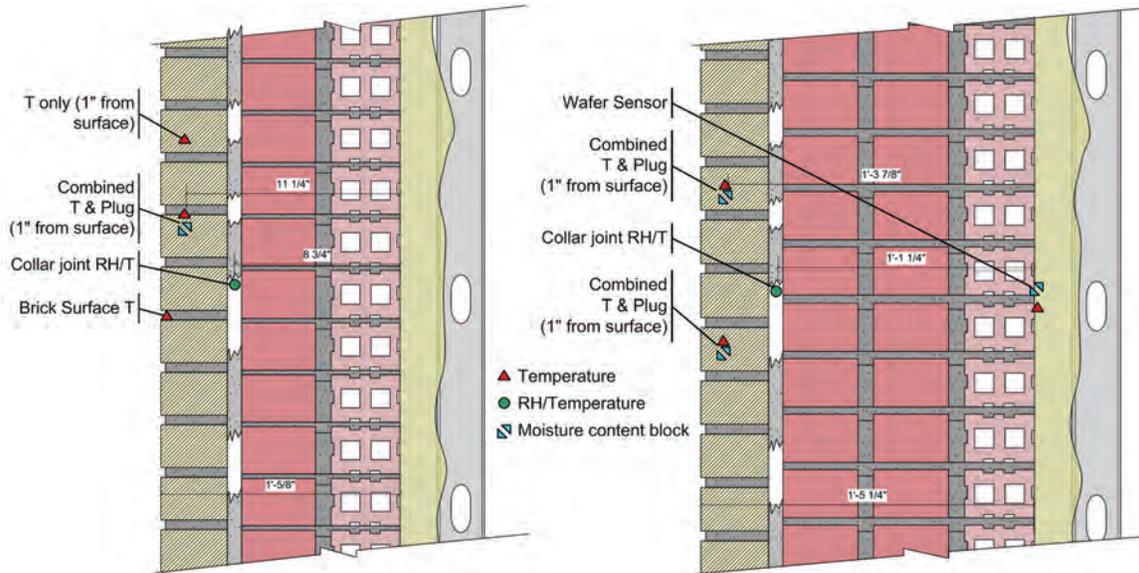
Figure 3 *Sensor package for "thin" wall (N1/S1) left; "thick" wall (N2/S2) right.*

Figure 4 *(Left) Installation of combined temperature and "plug" (wood cylinder) sensor; (middle) sensor encapsulated in clay for capillary contact; (right) boroscope image of installation hole.*

Sensor Arrangement and Data Acquisition System

A variety of sensors were embedded through the thickness of the test walls; the layout varies depending on wall configuration (Figure 3). The sensors included temperature sensors (±0.2°F [0.1°C] NTC thermistor), relative humidity sensors (thermoset polymer capacitive based sensors; ±3% between 10% and 90% rh), and "moisture content blocks." The latter sensors are wood-based relative humidity surrogate sensors, described in detail by Ueno and Straube (2008); the moisture content of the wood (eastern white pine) is measured via electrical resistance.

There are two configurations of moisture content blocks: the "plug" sensor (a cylindrical sensor, embedded in a hole drilled into the masonry) and the "wafer" sensor (a flat, thin rectangle of wood which measures conditions at an interface surface, such as between the insulation and the masonry wall). These surrogate sensors were chosen in lieu of relative humidity sensors due to (a) greater longevity in condensing or liquid water wetted environments, (b) greater resolution of bulk water wetting events, and (c) some indication of the accumulation of moisture (or storage) over time. Further information on these monitoring methods is provided in Straube et al. (2002).

Some sensors are duplicates, given the variation that can occur in conditions within a wall assembly. The uninsulated wall was wired with the same scheme as the "thick" wall.

Embedded sensors were installed from the interior, at holes drilled through the masonry to the appropriate layer (Figure 4, left). The holes were then sealed from the interior (and other layers/air spaces) using low-expansion foam. The plug sensors were encapsulated with clay before installation, to improve capillary contact between the sensor and the surrounding material (Figure 4, middle). An alternate installation method (not used here) is to inject a clay slurry into the hole;

this ensures consistent capillary contact, but adds an initial moisture signal to disaggregate from the wall behavior. The conditions of the installation hole were typically examined with a boroscope before sensor installation, to identify anomalies (Figure 4, right). The installation locations included in masonry joints (i.e., higher rainwater absorptivity), within the solid brick body, and intersecting with the air-filled brick cores (which could allow some drying). The lateral location of the sensors within the masonry wall could not be tightly controlled due to this "blind" (interior side) installation.

One caution when interpreting the results of the surrogate sensors is that their time response is very slow, based on Ueno and Straube (2008) and Wilkinson et al. (2009). Therefore, they would have difficulty resolving short-term (daily) rain events. Specifically, the sensors have an asymmetric response: slow response to increasing RH (adsorption/wetting), and fast response to decreasing RH (desorption/drying). However, the sensors are still useful to track seasonal trends when comparing wall assemblies.

A weather station was installed on the building's roof measuring temperature, relative humidity, wind speed and direction, horizontal rain, and horizontal solar radiation. Solar radiation sensors were mounted on the front and rear walls to directly measure radiation on the vertical surfaces.

Data are being collected by a measurement and control system installed in the service stairwell; data are measured at five minute intervals, and average values are recorded hourly. No battery backup for the data logger is provided; however, the unit has non-volatile memory, and resumes data collection after a power failure.

MONITORING RESULTS

Data have been collected from early October 2011 through early June 2013, providing over one and a half years of results. The intent is to collect data for a minimum of two years.

Boundary Conditions

Exterior and interior boundary conditions were recorded; exterior and interior temperatures are shown in Figure 5. Interior conditions were measured in the north-facing room, south-facing room, and the north-facing stairwell with uninsulated walls. North and south interior temperatures were typically controlled to the 70°F to 77°F (21°C to 25°C) range, but with some excursions to the high side in the south-facing room (likely due to solar gain and/or thermostat setup control issues). The stairwell was semi-conditioned (heating-only), with temperatures between interior setpoints and exterior temperatures.

Winter 2011–2012 conditions were exceptionally mild (4400 HDD Base 65°F [2440 HDD18°C] versus 5600 HDD65°F [3110 HDD18°C] climate normal). Winter 2012–2013 was closer to normal conditions (5400 HDD Base 65°F [3000 HDD18°C]).

Wintertime relative humidities have been exceptionally low, often in the 5%–15% range. Summertime measurements show control of interior relative humidity levels, typically in the 30%–50% range. When dewpoint temperatures are calculated (Figure 6), wintertime interior dewpoints are almost identical to exterior dewpoints, which might indicate an excessively high ventilation rate (or air leakage, less likely based on test results), low interior moisture generation, or a combination of both. Some dewpoint data are missing, due to failures of relative humidity sensors.

Figure 7 (left) shows driving rain, as calculated from Boston airport (KBOS) data, using methods described by Straube (2005). Site-measured weather station rainfall data appeared to be missing significant rainfall events, so it was not used in this analysis. The plot shows the cumulative driving rainfall for the monitored period. The test wall orientations are superimposed on the driving rain rosette for reference. The plot clearly shows that the test walls were not at the highest exposures to driving rain, and that the rear/project north side had much lower rainfall than the front/project south side.
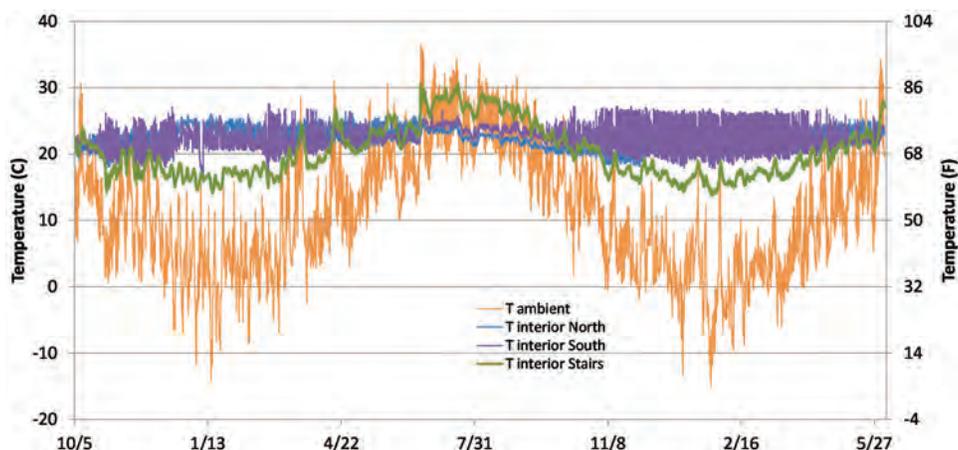
Figure 5 *Exterior and interior temperatures.*
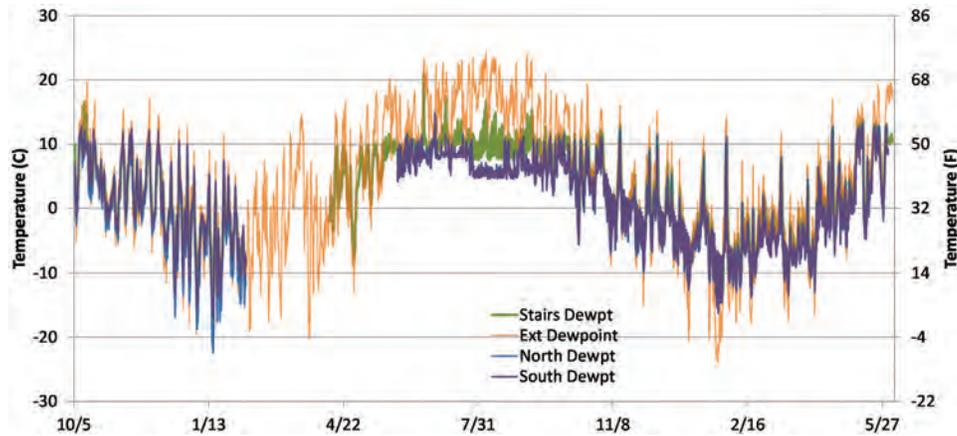
Figure 6 *Exterior and interior dewpoint temperatures.*
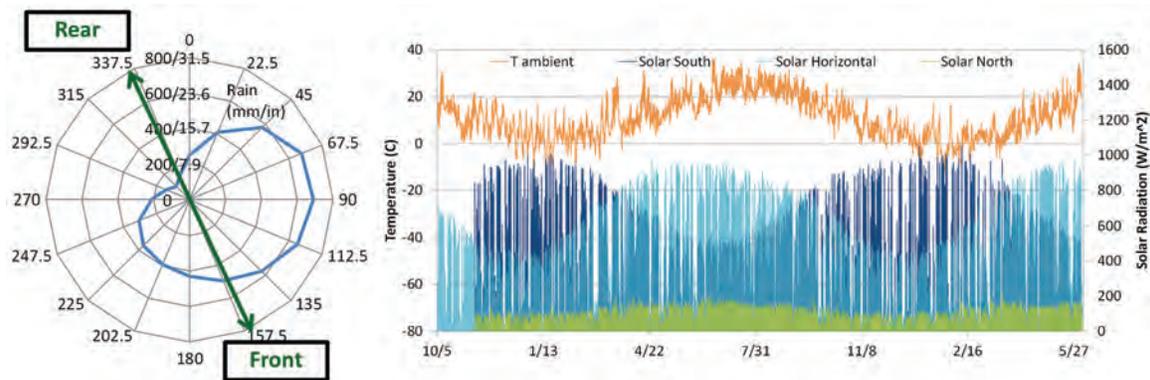
Figure 7 *(Left) Driving rain rosette in mm (in.) (calculated from Boston airport data), with building faces shown; (right) solar radiation at building for horizontal, north wall, and south wall.*

Solar radiation was plotted with exterior temperature for reference including horizontal, north wall, and south wall data (Figure 7 right). It shows the expected pattern of a seasonal rise and fall with higher solar gain on the south wall in wintertime (due to low sun angle). The north wall experiences consistently low solar gain (diffuse radiation only).

Temperature Measurements

Temperatures were measured through the thickness of the wall, including at the exterior surface, in the exterior brick wythe, in the collar joint (inboard of the exterior wythe), and at the masonry-insulation interface (see Figure 3). Selected temperatures for north-facing insulated walls are shown in Figure 8; it shows that the wall temperatures basically follow exterior conditions (within several degrees) regardless of position within the wall (albeit with some damping due to thermal mass, especially at the innermost wafer temperature).

The south-facing walls have much higher temperature peaks than the north-facing walls (due to solar gain), with peak temperatures over 104°F (40°C). However, coldest temperatures are roughly as low as on the north side, during night periods.

The north-facing uninsulated wall is markedly different from the north-facing insulated walls. Instead of tracking outdoor conditions, the temperatures fall in a range between indoors and outdoors, depending on position through the assembly thickness (Figure 9). The sensor at the interior surface of the masonry (but hidden by drywall) is roughly halfway between indoor and outdoor temperatures. The wintertime temperatures within the uninsulated masonry wall are warmer than the insulated case.

The temperature behavior of these walls is consistent with a steady-state calculation of the temperature gradient through the wall. In the uninsulated case, the masonry provides the majority of the insulation value of the wall, so the temperature drops gradually through the thickness of the masonry. In contrast, post-insulation, the interior insulation (spray foam) layer provides the majority of the insulation value in the wall. Therefore, the entire thickness of the masonry wall operates close to exterior temperatures.

In addition, the number of freeze-thaw cycles at several locations in the assembly was summed for the recorded data (Table 1). A freezing temperature of 23°F (–5°C) was used (as
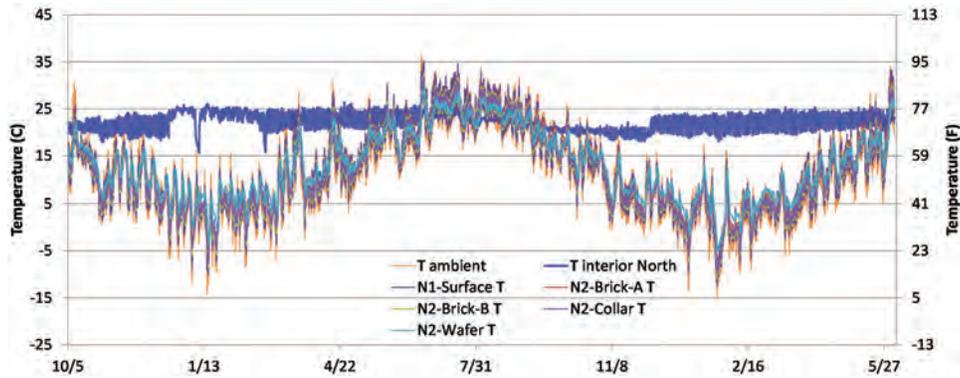
Figure 8 *North insulated wall representative temperatures, with interior and exterior temperatures.*
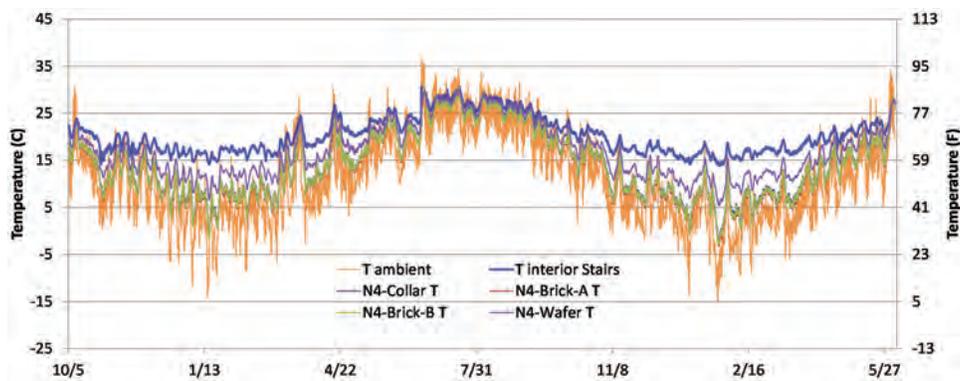
Figure 9 *North uninsulated wall representative temperatures, with interior and exterior temperatures.*

opposed to 32°F (0°C), which reflects the depressed freezing point within porous media (Straube and Burnett 2005), although even lower temperatures may be more appropriate. The number of ambient air cycles below the critical temperature is shown in Table 1 for reference.

Although ambient air temperature shows multiple sub-23°F (–5°C) cycles, only a fraction of them occur within the wall, due to thermal mass effects. The surface of the masonry wall experiences more cycling than inner portions ("collar joints"). Insulated north facing wall collar joints (N1, N2, and N3) have more cycles than uninsulated (N4) or south (S1) walls.

In order to provide greater differentiation between N4 and S1 (both zero counts in Table 1), the summed freezing cycles using a warmer temperature of 32°F (0°C) are shown in Table 2. The results are consistent with Table 1, but show that the collar joint of the uninsulated wall (N4) experiences the fewest cycles through 32°F (0°C). In addition, the count of freeze-thaw cycles in the north and south insulated walls (N1, S1) can be compared. At the surface, the south wall has a larger number of cycles, which is consistent with wintertime solar gain temperature cycling. But deeper in the wall (at the collar joint), the north wall has more cycles than the south wall.

Overall, these results should not be taken in isolation to indicate greater risk due to insulation retrofits. As described by Mensinga et al. (2010), freeze-thaw damage only occurs when freezing temperature cycles occurs while masonry moisture content is above S_{crit}; moisture behavior is discussed further below.

Moisture Plug (Brick Moisture) Measurements

The results from the plug surrogate relative humidity sensors placed in the exterior brick wythe were plotted; the graphs include calculated driving rain on the wall (in mm/h and in./h) and a dotted line showing the approximate equivalence of 100% rh (27%–32% wood moisture content, as calculated by previous calibration; see Ueno and Straube 2008).

The north-facing insulated wall responses (Figure 10) vary widely, and are not necessarily correlated with location. For instance, most sensors start within a similar band of moisture contents (MCs), but over the summer, the "thin" wall and one "false parapet" sensor dry down to 10%–15% MC (55%–80% rh equivalent). But other walls stay much wetter, and/or dry only at the end of the summer ("thick" wall sensors, N2). There was no indication that the "false parapet" sensors (N3) consistently experienced more wetting than other portions of the wall.

Most plug sensors show a response to some driving rain events; for instance, Hurricane Sandy (October 29, 2012) resulted in a major increase in moisture content across all sensors. However, some significant driving rain events did not result in a noticeable wetting response. This might be expected, given the complication of calculating and predicting driving rain on the face of a building in an urban environment. The general pattern for most of the north-facing sensors was in the 22%–35% MC range (93%–100% rh equivalent).

The south-facing sensors (Figure 11) had similar patterns; one "thick" wall sensor (S2-Plug B) showed "spiky" behavior closely matching driving rain events, while other sensors were less responsive. The general range for the south-facing sensors was dryer than the north-facing sensors, at

15%–28% MC (78%–100% rh equivalent). The moisture contents appear to rise higher in winter/spring 2013, which is not directly correlated to greater amounts of calculated driving rain.

The sensors in the north-facing uninsulated wall (Figure 12) have a markedly drier response than the insulated walls, typically in the range of 9%–13% MC (50%–70% rh equivalent). There is a slight seasonal rise and fall (greater moisture in winter), but the response is small compared to the insulated walls.

One puzzling aspect, though, is that there is no discernible response to any driving rain wetting events, unlike the insulated north- and south-facing walls. Looking at the installation (Figure 2), it seems plausible that the sensors have

Table 1. Number of Freeze-Thaw Cycles (Through 23°F [–5°C]) within Wall Assemblies

Location	Number of Occurrences	Location	Number of Occurrences
Exterior (Ambient Air)	34	N1 (Thin)-Collar Joint	8
		N2 (Thick)-Collar Joint	5
N1 (Thin)-Surface	11	N3 (Parapet)-Collar Joint	2
S1 (Thin)-Surface	12	N4 (Uninsulated)-Collar Joint	0
		S1 (Thin)-Collar Joint	0

Table 2. Number of Freeze-Thaw Cycles (Through 32°F [0°C]) within Wall Assemblies

Location	Number of Occurrences	Location	Number of Occurrences
Exterior (Ambient Air)	88	N1 (Thin)-Collar Joint	19
		N2 (Thick)-Collar Joint	21
N1 (Thin)-Surface	44	N3 (Parapet)-Collar Joint	6
S1 (Thin)-Surface	65	N4 (Uninsulated)-Collar Joint	4
		S1 (Thin)-Collar Joint	10
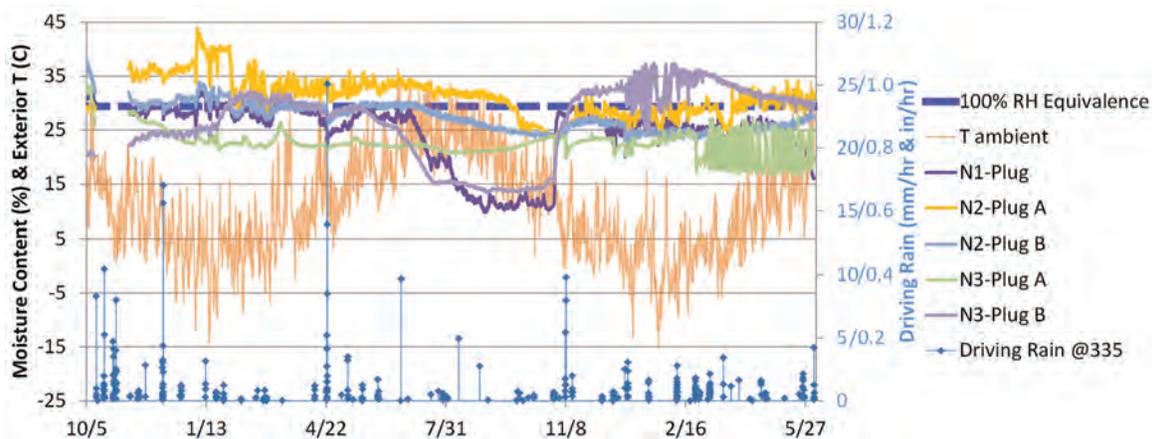
Figure 10 *North insulated wall plug sensor moisture contents with exterior temperatures and driving rain.*
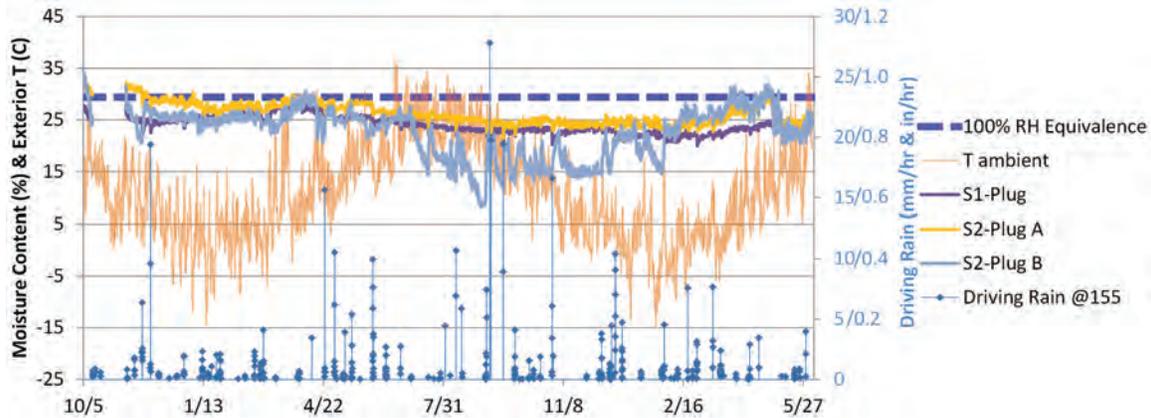
Figure 11 *South insulated wall plug sensor moisture contents with exterior temperatures and driving rain.*
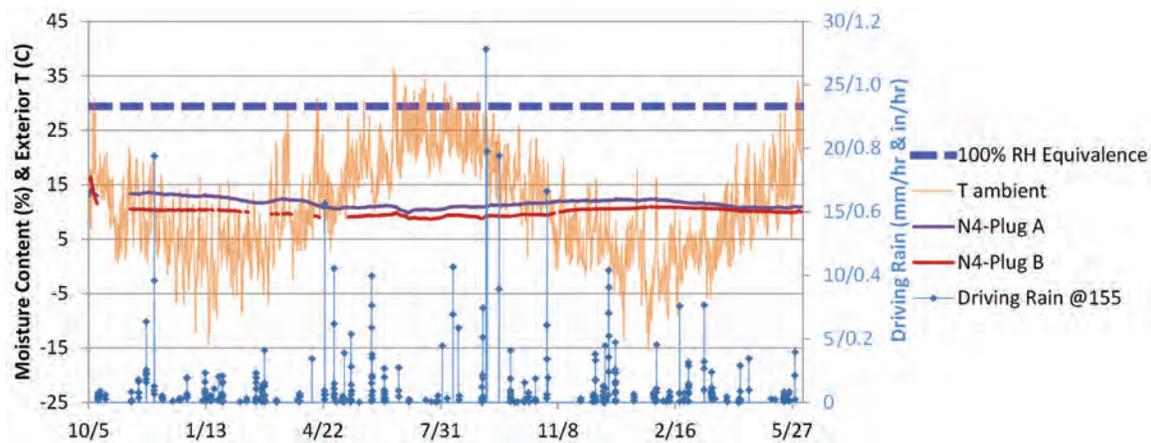
Figure 12 *North uninsulated wall plug sensor moisture contents with exterior temperatures and driving rain.*

been installed close enough to the exterior cornice detail that they are largely shielded from driving rain. This would explain both the lack of response as well as the exceptional dryness of the masonry wall. Overall, it is unclear how much of the sensor patterns can be attributed to the lack of thermal insulation, compared to the lack of rain deposition on the wall.

Although it should be a concern that the insulated walls are measurably wetter than the uninsulated wall, it is important to understand the mechanism of potential failure modes. The primary worry is freeze-thaw damage of the outer face of the masonry, which occurs when brick moisture contents exceed the critical degree of saturation (S_{crit}; see Mensinga et al. 2010). This topic is covered later in the synthesis of measured and simulation results.

Relative Humidity Measurements

Temperature and relative humidity sensors were placed in the "collar joint" region (between the outer brick wythe and the backup wall) of all of the test walls. However, there was a systemic failure of the relative humidity sensors after the first

winter, so the results are not presented here. The results were generally consistent with the surrogate humidity plug sensors: for instance, the north insulated walls remained at 100% rh for most of the monitored period. The south insulated wall was drier than the north insulated wall (70%–80% rh), and the uninsulated north had substantially lower RH levels than either insulated wall (45%–60%). When interpreting this data, it should be noted that relative humidity measurements do not resolve moisture contents in the high range needed to determine whether masonry is below or above critical degree of saturation (S_{crit}).

Moisture Wafer Measurements
(Masonry-Insulation Interface Conditions)

Temperature and surrogate relative humidity sensors (wafer sensors) were installed at the interior surface of the masonry to measure conditions at the insulation-masonry interface (Figure 13, left). The intent of these measurements is to capture the occurrence of interior-sourced moisture that may be transported by diffusion and condense on the cold ma-
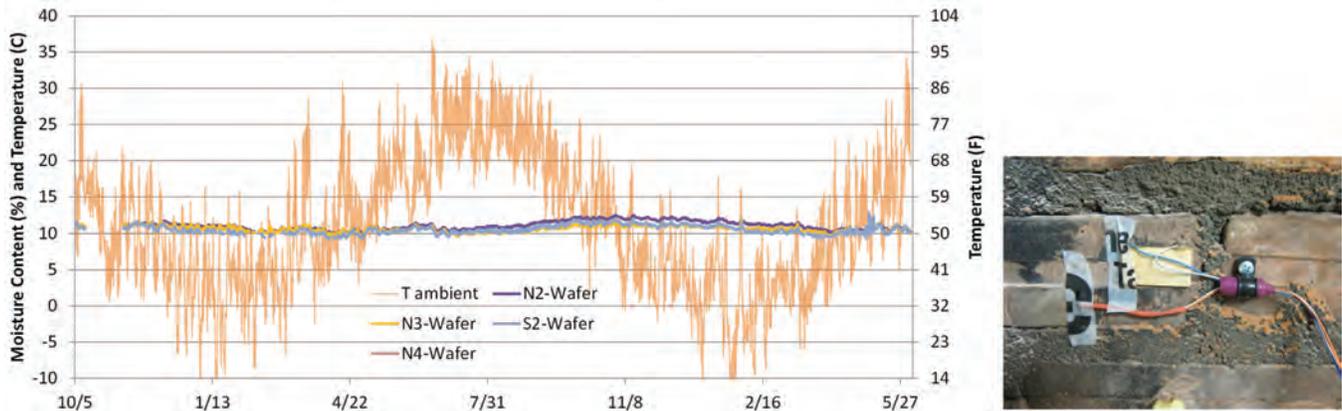
Figure 13 *(L) Moisture wafer results, with exterior temperature for reference; (R) example of wafer sensor.*

sonry surface during wintertime. This risk was considered greater due to the use of open-cell foam, which has higher vapor permeability than closed cell foam.

The measurements (Figure 13, left) remained in the 10%–13% MC range (50%–70% rh equivalent), which is a safe range for avoiding moisture-induced degradation of building materials. Before concluding that this retrofit wall assembly is safe from interstitial condensation, it must be noted that interior relative humidity levels were exceptionally low (5%–20%) during both winters, which reduces the risk of wintertime condensation.

The risk could also be assessed by comparing the temperature of the masonry-insulation interface to the interior dewpoint: during the winter, interior dewpoints were almost always below the interface temperature, which essentially eliminates condensation risks. These low dewpoints could be due to high ventilation rates, air leakage, low interior moisture generation, or a combination thereof. Overventilation due to the active beam heating and cooling system is suspected: a common problem is overspecifying primary airflow (beyond ventilation and latent load requirements) to meet space conditioning requirements (Livchak and Lowell 2012).

HYGROTHERMAL SIMULATIONS

Simulation Setup

One-dimensional hygrothermal simulations were run using WUFI 5.2 (IBP 2012); a variety of wall assemblies and the two orientations were simulated; the site-measured interior and airport weather data provided interior and exterior boundary conditions. Simulations were run for a period matching the monitored data (October 2011–May 2013).

Material properties for the masonry materials were taken from an outside masonry testing consultant's report on samples collected from the building (22 samples of four material types). Properties included dry density, capillary uptake, calculated porosity, and an estimate of the critical degree of saturation (S_{crit}). These values were used to modify existing materials in the WUFI database. The masonry consultant reported mortar consistent with Type N composition; the WUFI database Type N mortar was used. Open cell polyurethane foam from the WUFI database (based on ASHRAE 1018-RP data) was used (11.8 perms [670 ng/(Pa·s·m^2)]) for the 4.5 in. (116 mm layer).

A typical wall section is shown in Figure 14, which models the wall layers pictured in Figure 3; the image also shows the location of temperature/relative humidity monitors, which mostly correspond to site measurements.

The collar joint and the joint between the face and fill bricks were modeled as solid mortar; in reality, these joints are incompletely filled with mortar, with a variety of cracks and voids in the fill. In addition, the hollow clay block is shown as solid (as per the block's web condition), as opposed to having an air space (hollow core).

A sensitivity analysis was done in WUFI to determine whether replacing these mortar joints and clay block cores with air spaces would result in a significant difference in performance. A comparison was run between these two cases (no air spaces versus all air spaces): in the uninsulated wall, temperatures through the wall were identical. In the insulated wall, there was a small (at most 0.9°F [0.5°C]) difference; adding air spaces resulted in a colder outer wythe, due to thermally decoupling the face brick from the backup wall. In terms of moisture performance, replacing mortar with an air space eliminates capillary contact between the two layers, increasing risk for the wetted layer (e.g., exterior), and reducing risk for the non-wetted layer (e.g., backup wall). However, modeling showed a relatively small difference between these cases.

Simulation Results and Comparison to Measured Data

The modeled masonry temperatures generally followed the measured values: during the winter, the simulated brick and collar temperatures tracked several degrees colder than measured. One possible reason is that the "true" thermal conductance of the brick outboard of these sensors is lower than
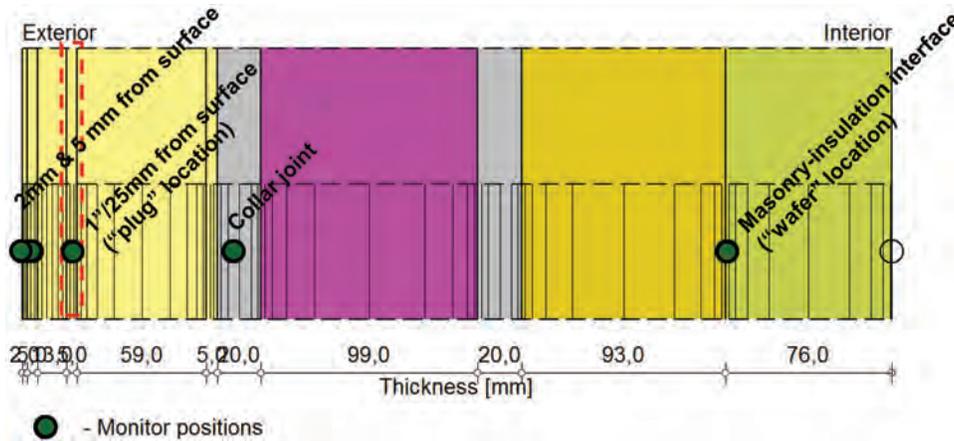
Figure 14 *WUFI model of Wall S1/N1 (insulated "thin" wall) with materials and monitor positions.*
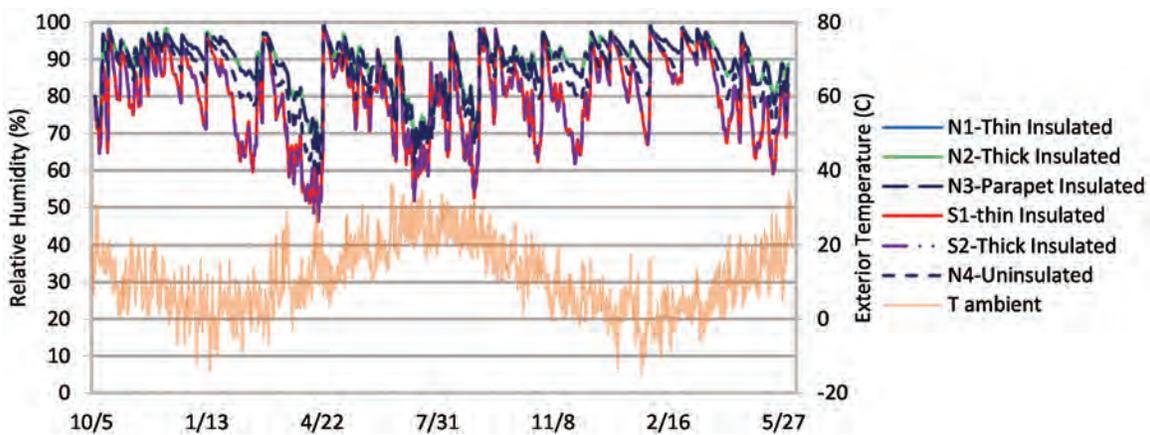
Figure 15 *Simulation brick layer 1 in. (25 mm) from exterior face relative humidity; exterior temperature for reference.*

in the model (i.e., the outboard brick assembly is more insulating than simulated). The brick may be less dense or thicker, the sensor may be located further away from the outside surface than modeled, or the presence of air voids around the sensors might reduce apparent thermal conductance. Similarly, the wafer temperatures tracked several degrees colder as well. This could be in part due to the brick conductivity and in part due to a conservative value for the open cell foam conductivity used in the model.

The modeled response of the outer layer of brick, 1 in. (25 mm) from the surface (layer highlighted in Figure 14) was examined closely as its position corresponds to the plug sensor in the monitored wall. The response is plotted in Figure 15 in terms of relative humidity (as opposed to moisture content) to allow a simpler comparison to the plug sensor response.

The response of the model is a common pattern seen in hygrothermal simulations of mass masonry assemblies. Moisture conditions rise sharply (to the 90%–100% range) in response to driving rain events and then dry slowly over time. Further driving rain events cause additional jumps in RH.

During the winter, south-facing walls dry at a faster rate than the north-facing walls, and the uninsulated north-facing wall dries faster than the insulated walls.

However, the simulated behavior contrasts sharply with the measured data (see Figures 10, 11, and 12). For instance, very few driving rain events caused discrete responses in measured data but were evident in the simulation. The general trend in the measured data was consistently high humidity levels in the wintertime, followed by drying (in some cases) in the summertime.

In addition, the measured moisture levels mostly fell into overlapping bands that correlated with the wall category. The insulated north walls were consistently the wettest, the south-facing insulated walls the driest, and the north-facing uninsulated wall somewhere in between.

Another comparison is to the relative humidity levels at the collar joint between the face brick and the backup wall. The simulated response at this layer is shown in Figure 16. The order of the responses is consistent with the order seen in the measured plug data. In addition, the RH levels are roughly

consistent with the limited measured collar joint RH data, although measured RHs in the uninsulated wall (N4) are drier (45%–67% rh) than in the simulation (80%–85% rh). This difference may be ascribed to the rain sheltering caused by the overhanging cornice detail at the N4 monitoring location.

Simulation results for the relative humidity at the masonry-insulation interface (equivalent to the wafer placement) are shown in Figure 17. The simulation results show RH levels in the 65%–85% range, with variations correlating with outdoor temperature. In comparison, the measured data showed a more damped response, as well as drier conditions; the measurements centered at 50%–70% rh equivalent (10%–13% MC).

Part of the difference between simulation and measured responses may be due to the slow response of the wood-based surrogate humidity sensors. However, the cycles seen in these simulations are not simple diurnal variations; they are variations over the course of multiple days. It is plausible that the simulation does not correctly capture the vapor permeance characteristics of the wall assembly installed inboard of the masonry wall (open-cell foam and painted gypsum board).

The simulations also examined the moisture content of outer brick layers, to determine freeze-thaw risks. Assuming typical rain exposure levels, and S_{crit} values as presented in the masonry consultant's report, simulation peak moisture contents (under 3% by mass) never approached levels which would cause freeze-thaw damage (5%–7% by mass). This held true for the thin outermost layers, centered at 0.1 in. (2 mm) and 0.2 in. (5 mm) from the surface. Furthermore, the comparison to measured data showed that the simulation was conservative, assuming colder temperatures and more moist conditions.

ANALYSIS AND SYNTHESIS

Both the measured data and the modeling indicate that insulation of the masonry wall results in colder temperatures (through the thickness of the wall) and higher moisture levels. These changes are entirely expected given the fundamental physics. Although the north-facing insulated walls have higher moisture contents than the uninsu-
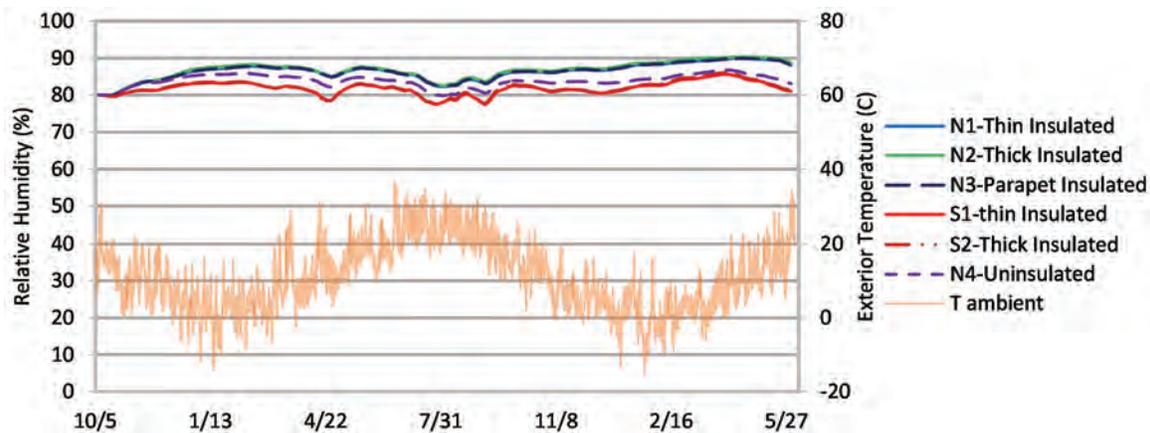
Figure 16 *Simulation collar joint (mortar layer) relative humidity; exterior temperature for reference.*
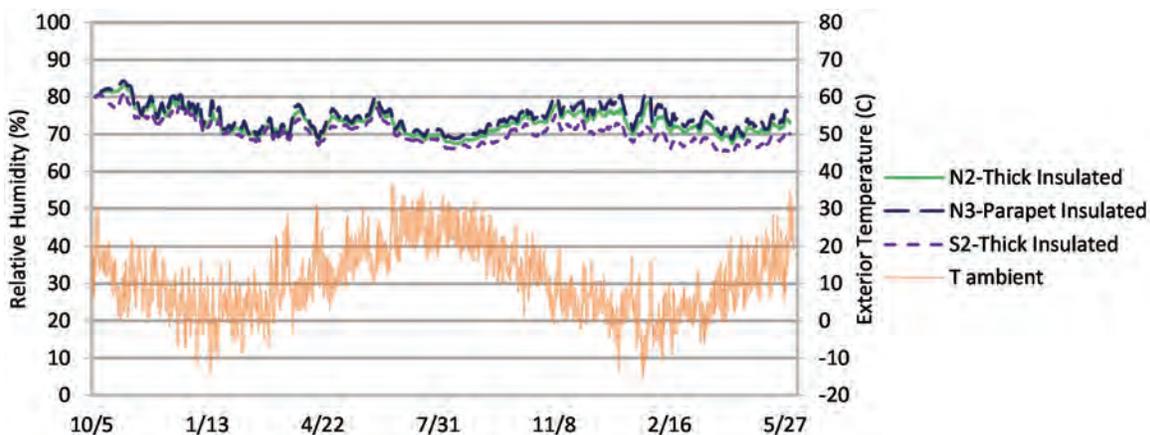
Figure 17 *Simulation wafer (masonry-insulation interface) relative humidity; exterior temperature for reference.*

lated north-facing wall, this difference might reflect both insulation levels and rain exposure, due to shielding by the overhanging cornice.

Although temperature agreement between the model and measured data was good, there were significant differences in moisture responses. Part of this can be ascribed to the properties of the wood-based humidity surrogate sensor; they are unlikely to indicate short-term humidity fluctuations. The difference might also be due to rain exposure: driving rain on the walls was calculated based on measured horizontal rain and wind data. Localized effects—in particular, surrounding buildings—can have an effect on rain deposition. Driving rain gauges on the exterior walls, near the monitored locations, would reduce the uncertainty of this boundary condition. A potential confounding factor is that the capillary contact between the plug sensors and the surrounding masonry may not be consistent from installation to installation.

Another potential cause of anomalies is the construction of built-up mass masonry wall assemblies. In a light wood frame wall, thermal and moisture anomalies can typically be characterized (e.g., framing members, air leakage at sheathing joints or roof-floor connection), and monitoring locations can be chosen to avoid them (e.g., mid-height/center of a stud bay). In contrast, in a mass masonry assembly built of multiple layers and materials (such as these walls), the assembly has a network of voids (incompletely filled mortar joints, brick cores, clay block cores) and capillary active cracks which can result in redistribution of moisture by bulk water drainage, capillarity, air movement, or vapor diffusion. These types of anomalies would be difficult to capture in a one-dimensional hygrothermal simulation. For instance, these networks could result in drainage of bulk water away from one portion of the wall, resulting in concentration in another portion (Laska 1997). This is consistent with the varying responses of plug sensors that are nominally in the same type of wall (i.e., duplicated sensors). Some sensors show strong wetting and drying responses, while others show minimal response to outdoor conditions.

As discussed by Wilkinson et al. (2009), the plug sensors are not suitable for determining whether masonry layers are reaching moisture contents above S_{crit}. One reason is that S_{crit} is a high moisture content (high fractions of saturation), which is above the resolution range of this sensor. An example is given below in Table 3, showing the relative humidity, equivalent wood moisture content (based on the sorption isotherm and correlated by Ueno 2008), and equivalent brick moisture content (for the face brick material properties measured at this site).

The table shows that although the plug sensors are useful for general trending data of moisture levels, it cannot resolve the high moisture contents that are critical for freeze-thaw performance. However, the sensor can provide an accurate indication that the wall is below the critical moisture levels associated with freeze-thaw damage.

Table 3. Correlation of Relative Humidity, Wood Moisture Content, and Brick Moisture Content

RH, %	Wood MC (Weight %)	Face Brick MC (Weight %)	Notes
50	~9	0.02	Lower limit of resolution for wood surrogate sensors
80	16	0.09	Reference water content (W_{ref} or W_{80})
90	20	0.19	
95	24	0.38	
100	29+	4.3	Free water saturation (W_f)
100	n/a	5–7	Critical degree of saturation (S_{crit}) for face brick samples

Another sensor issue is that freeze-thaw failures typically occur when S_{crit} is exceeded in a thin layer, roughly ~1/16 to 1/8 in. (1.6 to 3 mm) from the surface. This is the layer that is (a) sufficiently cold to experience freeze-thaw cycling (near the surface), (b) experiences outdoor precipitation events, but (c) has limited drying to the exterior (unlike the surface layer), resulting in the highest moisture contents. These sensors do not have spatial resolution to distinguish this type of thin layer.

This raises the question, though, of whether there are any effective in-situ measurements that can measure the moisture content of masonry materials in the S_{crit} range. Physical removal of samples by cutting (for gravimetric testing) will result in localized heating, and thus a change in moisture content. An easily removable surface sample will have capillary contact dissimilar to the body of the wall. Künzel and Holm (2009) describe the use of in-situ nuclear magnetic resonance (NMR) scanning to obtain one-dimensional moisture profiles in mass masonry walls. This method is promising, but limitations include high equipment cost, limited penetration (0.4–0.8 inches [10-20 mm]), and interference from embedded ferrous materials. In addition, it may be worthwhile to perform laboratory tests of handheld impedance-based moisture meters or similar instruments to determine whether they can differentiate between the moisture contents in the S_{crit} range.

EXTERIOR INFRARED OBSERVATIONS

In addition to the measured data and hygrothermal simulations, cold-weather infrared thermography was conducted at the building in January of 2012; the exterior temperature at the time of these measurements was roughly 25°F (–4°C). The front/south elevation is shown in Figure 18.

There is conspicuous evidence of thermal bridging through the exposed floor slab edges. Due to the construction of the building, interior insulation of the masonry walls does not address the thermal bridging through the slabs (including
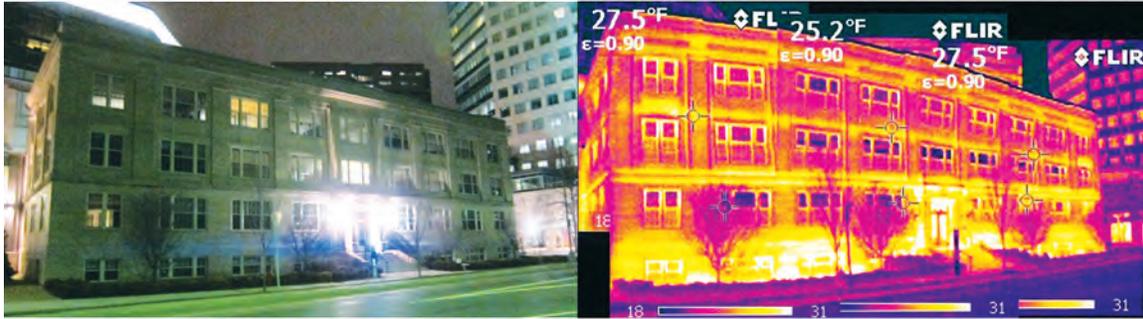
Figure 18 *Front (south) elevation visual and infrared images (composite infrared image). There is a significant thermal anomaly (indicating heat loss) at the entryway; this is consistent with the heated but uninsulated (due to historic finishes) entryway, and possibly air leakage around the entry doors.*

the roof slab) cast into the structure. The effect of thermal bridging on overall thermal performance of the wall can be approximated using a parallel paths method: assuming R-10.6/RSI 1.9 (over a 10 ft [3.0 m] wall), and R-3/RSI 0.5 (for a 1 ft [0.3 m] floor slab), this results in an overall R-8.6/RSI 1.5. The penalty for thermal bridging through the uninsulated slab edge becomes greater as wall insulation levels are increased. Calculations using linear transmittance (Ψ) values for similar assemblies from Morrison Hershfield (2011) gave comparable results, of R-7.3/RSI 1.3 for a nominal R-10 wall (73% effective), and R-13.3/RSI 2.3 for a nominal R-25 wall (53% effective).

There is a significant thermal anomaly (indicating heat loss) at the entryway; this is consistent with the heated but uninsulated (due to historic finishes) entryway, and possibly air leakage around the entry doors.

There is also a significant thermal anomaly at grade, with warmer temperatures at the half-buried floor than at the wall above. The basement walls at the front of the building are shown as insulated on the plans. The thermal anomaly might reflect the thermal connection between the wall and the surrounding soil. Based on previous measurements at multiple sites (Ueno et al. 2007), soil temperatures often stay above freezing (32°F [0°C]) even during extended freezing or sub-freezing weather, due to the latent heat of fusion of the bound water in the soil. The warmer soil temperatures tend to keep interior-insulated foundation walls warmer, even above grade. The surface temperatures observed at the front of the building are consistent with this phenomenon.

Some windows appear as low temperature surfaces; however, this should not be interpreted as a lack of heat loss (i.e., good insulation value). Instead, the cold surface temperatures are due to reflection of the cold night sky temperatures from the glass to the infrared camera.

The rear or north elevation clearly shows thermal bridging at the slab edges (Figure 19). In addition, a comparison can be drawn between the uninsulated wall (stairwell, with lights on; third bay from left, highlighted in yellow) and the insulated walls. Although the uninsulated wall has arguably warmer exte-

rior surface temperature, the two walls are very close in temperature, as would be predicted by a steady-state thermal gradient analysis. However, another confounding factor is different interior setpoints of 76°F (25°C) insulated north room and 59°F (15°C) uninsulated stairwell. The difference in setpoints is also consistent with the temperature difference between the window frames in the insulated and uninsulated portions.

In addition, there is a large thermal anomaly at the rear elevation curtain wall (signature stairwell) intersection with the masonry wall; this is consistent with an air leak between the masonry and curtain wall conditions. This appears to be a localized air leak at a specific detail; the body of the building shows no evidence of significant distributed air leakage.

CONCLUSIONS

The measured data from this mass masonry building retrofitted with interior insulation indicates that the masonry wall experiences colder temperatures than uninsulated walls, as would be expected. Monitoring also indicates that the insulated wall experiences higher moisture contents; however, this might reflect both the insulation retrofit and rain exposure at the sensor location. In addition, the moisture measurements in the walls varied in nominally identical wall sections: some sensors measured seasonally steady moisture levels, while others measured wetting responses consistent with driving rain events, followed by drying in warmer/drier conditions.

Hygrothermal simulations of the wall assemblies show good correlation to temperature measurements; however, there were significant differences in the moisture responses. These differences may be due to sensor response, driving rain exposure, or anomalies within the mass masonry wall assembly (redistribution of moisture due to voids and cracks).

The hygrothermal simulations indicate a low risk of freeze-thaw damage, based on predicted brick moisture content levels and insulation levels. The installed sensors cannot resolve moisture contents in the high range (critical degree of saturation or S_{crit}) at which freeze-thaw damage occurs. However, these instruments indicate seasonal trends of wetting and drying.
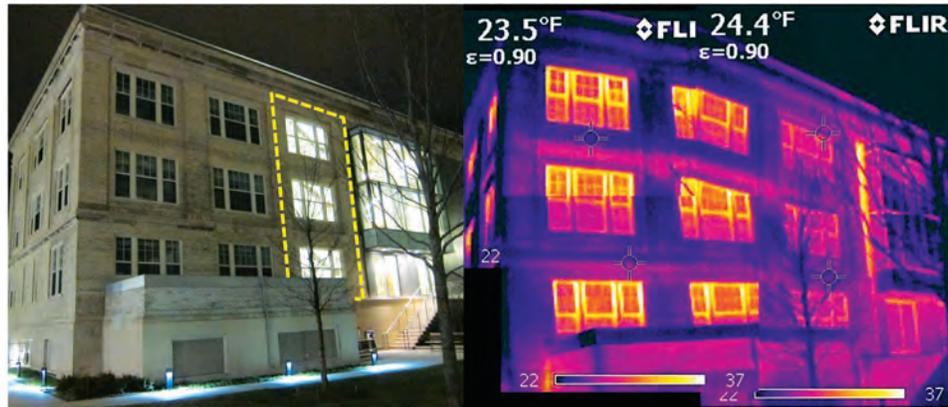
Figure 19 *Rear (north) elevation visual and infrared images (composite infrared image) with uninsulated stairwell wall high-lighted.*

Although the measured moisture levels were highly variable, and did not have high correlation with modeled results, it still may be useful to install instrumentation in other mass masonry buildings retrofitted with interior insulation to gain understanding of the variables that affect the results. Direct measurement of driving rain on the instrumented wall surface may reduce the uncertainty.

In future work on insulated mass masonry buildings, the assessment of water shedding and water concentrations on the exterior face and improving the water shedding details are the key requirements before considering interior insulation. Material property testing and hygrothermal simulations are useful for assessing the risk in a more rigorous manner, based on localized climate and assembly type. Site load monitoring (driving rain, climate conditions) and building assembly monitoring are also useful tools—albeit more costly, intrusive, and time consuming—to consider in critical cases.

ACKNOWLEDGMENTS

REFERENCES

ASHRAE. 2009. *ASHRAE Handbook-Fundamentals*. Atlanta, GA: ASHRAE.

ASTM. 2012. *ASTM Standard C 67-12, Standard Test Methods for Sampling and Testing Brick and Structural Clay Tile*. West Conshohocken, PA: American Society for Testing and Materials.

ASTM. 2008. *ASTM Standard C 666-03, Standard Test Methods for Resistance of Concrete to Rapid Freezing and Thawing*. West Conshohocken, PA: American Society for Testing and Materials.

IBP. 2012. WUFI (Wärme und Feuchte instationär [Transient Heat and Moisture]), Version 5.2. Fraunhofer Institute for Building Physics IBP, Holzkirchen, Germany.

Fagerlund, G., 1977. The critical degree of saturation method of assessing the freeze/thaw resistance of concrete, *Journal of Structures and Materials,* 10(58):217–229.

Kosny, J., and J.E. Christian. 1995. Reducing the Uncertainties Associated with Using the ASHRAE Zone Method for R-value Calculations of Metal Frame Walls. *ASHRAE Transactions* 1995 v.101, Pt 2. Atlanta, GA: ASHRAE.

Künzel, H. and A. Holm. 2009. Moisture Control and Problem Analysis of Heritage Constructions. Congreso de Patologia y Rehabilitacao de Edifícios (PATORREB) 2009, pp.85–102.

Laska, W. 1997. Understanding Collar Joints. *Magazine of Masonry Construction* October, 1997. Chicago, IL: Hanley Wood Business Media.

Livchak, A., and C. Lowell. 2012. "Don't Turn Active Beams Into Expensive Diffusers" *ASHRAE Journal* vol. 54; pp. 52–60. Atlanta, GA: ASHRAE.

Lstiburek, J.W. May 2010. Building Sciences: Thick as a Brick. *ASHRAE Journal* vol. 52; pp. 50–56. Atlanta, GA: ASHRAE.

Mensinga, P., J. Straube, and C. Schumacher. 2010. Assessing the Freeze-Thaw Resistance of Clay Brick for Interior Insulation Retrofit Projects, *Performance of the Exterior Envelopes of Whole Buildings XI*. Atlanta, GA: ASHRAE.

Morrison Hershfield. 2011. Thermal Performance of Building Envelope Details for Mid- and High-Rise Buildings (ASHRAE Research Project 1365-RP) Report No. 5085243.01. Morrison Hershfield, Vancouver, BC.

Straube, J.F., Onysko, D., and Schumacher, C.J. 2002. Methodology and Design of Field Experiments for Monitoring the Hygrothermal Performance of Wood Frame Enclosures, *Journal of Thermal Env. & Bldg. Sci.*, Vol.26, No.2—October 2002. Thousand Oaks, Calif.: SAGE Publications.

Straube, J.F., and Burnett, E.F.P., 2005. *Building Science for Building Enclosure Design*, Building Science Press: Westford, MA.

Straube, J.F., and C.J. Schumacher. 2007. Interior Insulation Retrofits of Load-Bearing Masonry Walls in Cold Climates. *Journal of Green Buildings* 2(2):42–50.

Straube, J.F., K. Ueno, and C.J. Schumacher. 2012. Measure Guideline: Internal Insulation of Masonry Walls. Straube, Washington, DC: Building America Building Technologies Program, Office of Energy Efficiency and Renewable Energy, U.S. Department of Energy. www.nrel.gov/docs/fy12osti/54163.pdf

Ueno, K., C. Schumacher, and J. Straube. 2007. Field Monitoring and Hygrothermal Modeling of Interior Basement Insulation Systems, *Performance of the Exterior Envelopes of Whole Buildings X.* Atlanta, GA: ASHRAE.

Ueno, K., and Straube J. 2008. Laboratory Calibration and Field Results of Wood Resistance Humidity Sensors, *Proceedings of BEST 1 Conference*, Minneapolis, June 10–12, 2008.

Wilkinson, J., D. DeRose, J.F. Straube, and B. Sullivan. 2009. Measuring the Impact of Interior Insulation on Solid Masonry Walls In A Cold Climate. *Proceedings of Canadian Building Science & Technology Conference*, Montreal, pp. 97–110.